Phys. Status Solidi A **206**, No. 12, 2737–2742 (2009) / **DOI** 10.1002/pssa.200925276

physica status solidi a
www.pss-a.com
applications and materials science

Amorphous films of tris(8-hydroxyquinolinato)aluminium: Force-field, morphology, and charge transport

Alexander Lukyanov[*,1], **Christian Lennartz**[**,2], **and Denis Andrienko**[***,1]

[1] Max Planck Institute for Polymer Research, Ackermannweg 10, 55128 Mainz, Germany
[2] BASF SE, GVC/E-B009, 67056 Ludwigshafen, Germany

Received 29 May 2009, revised 1 July 2009, accepted 9 July 2009
Published online 12 August 2009

PACS 36.20.Ey, 72.80.Le, 61.30.−v

* Corresponding author: e-mail lukyanov@mpip-mainz.mpg.de, Phone: +49 6131-379 149, Fax: +49 6131-379 100
** e-mail christian.lennartz@basf.com
*** e-mail denis.andrienko@mpip-mainz.mpg.de

The effect of the force-field parameters on the morphology and charge dynamics is assessed for amorphous films of tris(8-hydroxyquinolinato)aluminium. Two force-fields are used for non-bonded parameters, OPLS and Williams 99, whereas bonded interactions are obtained from first-principles calculations. By comparing densities and glass transition temperatures we conclude that the OPLS-based force field provides a better description of the amorphous morphology. At the same time, the difference in molecular packing does not significantly affect the distribution of charge hopping rates or charge carrier mobility.

1 Introduction Tris(8-hydroxyquinolinato)aluminium (Alq_3, Fig. 1a) is a commonly used organic semiconductor with a higher electron than hole mobility [1]. The first organic light emitting diodes were made with Alq_3 and since then it has played the role of a 'guinea pig' compound in organic electronics [2]. The distinctive properties of Alq_3 are its green light emission and good electron mobility. It is also used as a host material for emissive dopants of lower emission energy.

In organic semiconductors both emission and charge transport properties are extremely sensitive to the material morphology. The latter can be controlled by an appropriate processing or compound derivatization. Understanding the link between the structure, morphology, and macroscopic properties of organic compounds is the first step towards their rational design [3].

In spite of numerous experimental studies, there were only two theoretical/computational attempts to relate the morphology of amorphous Alq_3 to its charge carrier mobility [4, 5]. In [4] the rigid-body approximation for the intramolecular structure was used together with the non-bonded parameters taken from the Dreiding force field. Approximate force constants for bonded parameters and non-bonded parameters of the Williams 99 force field were used in [5]. In both cases neither the force field nor the generated amorphous morphology was checked against the experimental data, and its characterization was reduced to pair correlation functions and density at ambient conditions.

In this paper, we first derive bonded parameters for the Alq_3 molecule using first-principles potential energy scans. Second, we compare Optimized Potentials for Liquid Simulations (OPLS) and Williams 99 force-fields to each other as well as to the available experimental data. Finally, we calculate distributions of charge transfer integrals and simulate charge dynamics for both morphologies.

2 Force-field parameters Force-field refinement can be split into several steps: (i) determination of partial charges; (ii) calculation of the force-field parameters for the bonded interactions; (iii) parameterization of the non-bonded interactions.

Partial charges were obtained from electrostatic potentials using a grid based method (CHELPG) [6] after the geometry optimization of a meridional Alq_3 isomer in vacuum (Fig. 1b) using B3LYP (Becke, three-parameter, Lee-Yang-Parr) functional and 6-311g(d) basis set. The corresponding dipole moment was $d = 4.4$ D. The DFT results were checked against MP2 calculations with

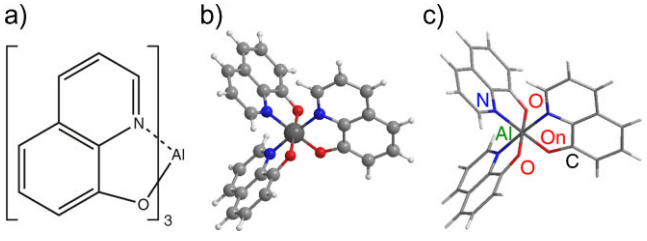

Figure 1 (online color at: www.pss-a.com) (a) Chemical structure of tris-8(hydroxyquinoline aluminium) (Alq_3), (b) meridional isomer of Alq_3, (c) atom labeling used to show the distributions of angles and dihedrals.

6-311g(d) basis set, for which the dipole moment is 5.4 D. No substantial differences were noticed with either B3LYP or MP2 charges used. All results reported here were, therefore, performed with charges based on calculations using B3LYP functional.

Bonded interactions were parameterized by matching the first-principle potential energy scans with the corresponding force-field based scans [7–9]. Note that the meridional isomer of Alq_3 is not symmetric, for example oxygen–aluminium–oxygen angle for O–Al–O is different from On–Al–O, as shown in Fig. 1c. The same holds for the dihedrals O–Al–O–C and On–Al–O–C. To simplify the force field we assumed that similar angles and dihedrals have the same parameters, i. e. all oxygens and all nitrogens have the same atom types. The equilibrium values of bonds, angles, and dihedrals were taken from the geometry-optimized meridional isomer in vacuum. The potential energy scans for the angles and dihedrals of interest were performed with GAUSSIAN 03 program [10] using B3LYP functional and 6-311g+(d,p) basis set. The results, together with the fits based on the atomistic force-field are shown in Fig. 2. The resulting force-field constants are summarized in Table 1. These constants are used to calculate angle and dihedral potentials using the following expression: $V(r) = \frac{1}{2}k_\theta(\theta - \theta_0)^2$.

Table 1 Bonded interactions parameters, obtained using the fitting described in the text.

degree of freedom	constant k_θ, (kJ mol^{-1} rad^{-2})
angle C–O–Al	500
angle O–Al–O	300
improper dihedral Al–O–C–C	30
improper dihedral On–Al–O–C	80

The Lennard–Jones parameters for all atoms were taken either from the OPLS [11] or Williams 99 [12] force field. Note that the OPLS force field uses the Lennard–Jones (12-6) potential while Williams 99 is based on the Buckingham potential, $V(r) = A\exp(-Br) - \frac{C}{r^6}$. The only difference between the two functional forms is the repulsive part, and one can refit the Buckingham potential with the Lennard–Jones one, which also results in a speed up of about 2.5. The non-bonded force field parameters are summarized in Table 2. The two force fields are compared in Fig. 3. One can see that the binding energy for nitrogen and oxygen is much bigger for the OPLS than Williams 99 force field and should result in a more dense molecular packing. Aromatic carbons have similar parameters.

To validate the OPLS-based force field we first studied distributions of angles and dihedrals of a single meridional isomer in vacuum. Two approaches were used: (i) NVE run of a single meridional isomer using the derived force field (at 300 K); (ii) Car–Parrinello molecular dynamics simulations [13] of the same isomer using the dispersion-corrected BLYP functional [14]. The final distributions are compared in Fig. 4 and agree reasonably well with each other.

To further verify the derived force field, we studied amorphous morphologies of Alq_3. The systems were prepared by first arranging the molecules on a cubic lattice with the density adjusted in order to avoid molecular overlaps and then equilibrating at 700 K in an NPT ensemble, with a velocity rescaling thermostat and the Berendsen barostat, and finally cooling down to room temperature.

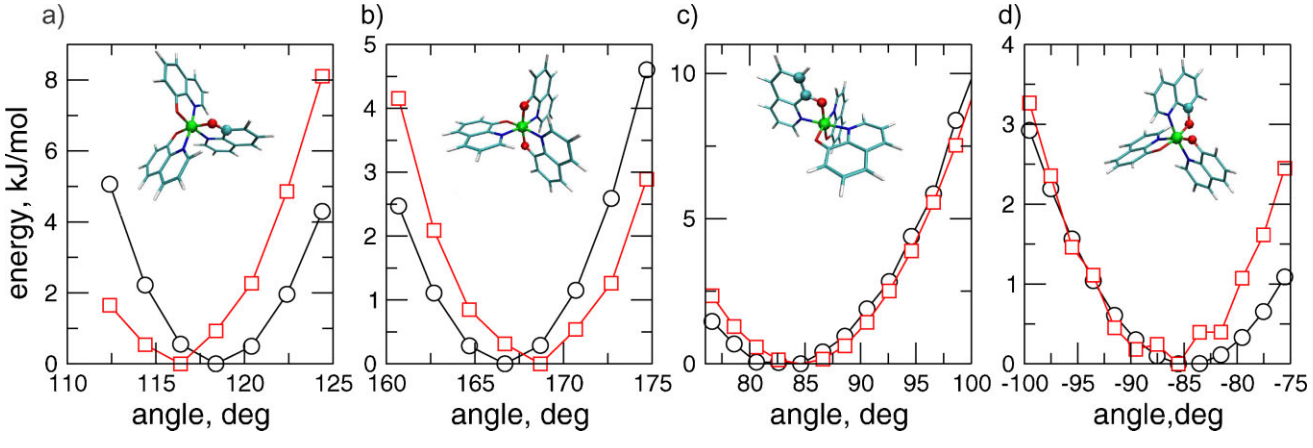

Figure 2 (online color at: www.pss-a.com) B3LYP/6-311+g(d,p) energy scans (circles) together with fits using OPLS force field (squares) for (a) C–O–Al, (b) O–Al–O, (c) Al–O–C–C, (d) On–Al–O–C angles and dihedrals. Insets illustrate the corresponding degrees of freedom.

Table 2 Non-bonded parameters of OPLS and Williams 99 force fields used in our simulations. For comparison, we also give the effective Lennard–Jones parameters obtained by fitting Buckingham potential of Williams 99 force field.

atom	OPLS		W99 fitted		W99		
	σ (nm)	ε (kJ/mol)	σ (nm)	ε (kJ/mol)	A (kJ/mol)	B (nm^{-1})	C ($kJnm^6/mol$)
carbon	0.355	0.29288	0.348873	0.263802	270363	36.0	0.00170173
hydrogen	0.242	0.12552	0.277899	0.107032	12680	35.6	0.00027837
oxygen	0.296	0.87864	0.305762	0.428992	284623	39.6	0.00128587
nitrogen	0.325	0.71128	0.327197	0.282361	102369	34.8	0.00139815

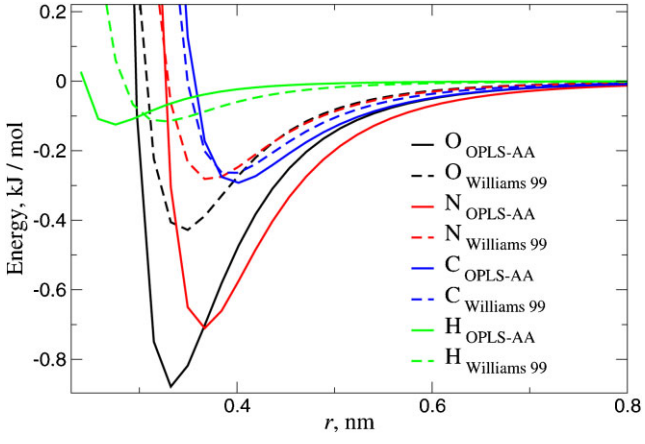

Figure 3 (online color at: www.pss-a.com) Non-bonded interactions between all atom types for the OPLS and Williams 99 force fields. OPLS force field has bigger binding energies for N and O.

All simulations were performed using the GROMACS package [15]. Note that two alternative ways of system preparation were reported previously. The first one based on the Monte Carlo algorithm mimicking the film deposition process [4], is limited to rigid molecules. The second based on a compression of a simulation box of a randomly positioned molecules at low density [5] is sensitive to the compression rate and often results in voids.

To monitor the equilibration dynamics we calculated relaxation times from the correlation functions for the rotational molecular motion as well as mean squared displacement (MSD) of their translational motion. Both are shown in Fig. 5a and b for a set of temperatures. Figure 5a and b indicate that systems can be equilibrated at 700 K after about 1 ns run, which is the time needed for the center of mass of a molecule to travel a distance comparable to its size. In addition, after this period of time molecular orientations are fully uncorrelated. At lower temperatures significantly longer runs are required. Therefore, to prepare large-scale morphologies, we annealed our systems at 700 K and then cooled them down to the desired temperature.

To compare molecular packing in amorphous morphologies generated with the OPLS and Williams 99 force-fields, we calculated two radial distribution functions, which are shown in Fig. 6a and b. One can see that different *bonded* parameters used in this work and [5] do not significantly change the radial distribution function. Note that, however,

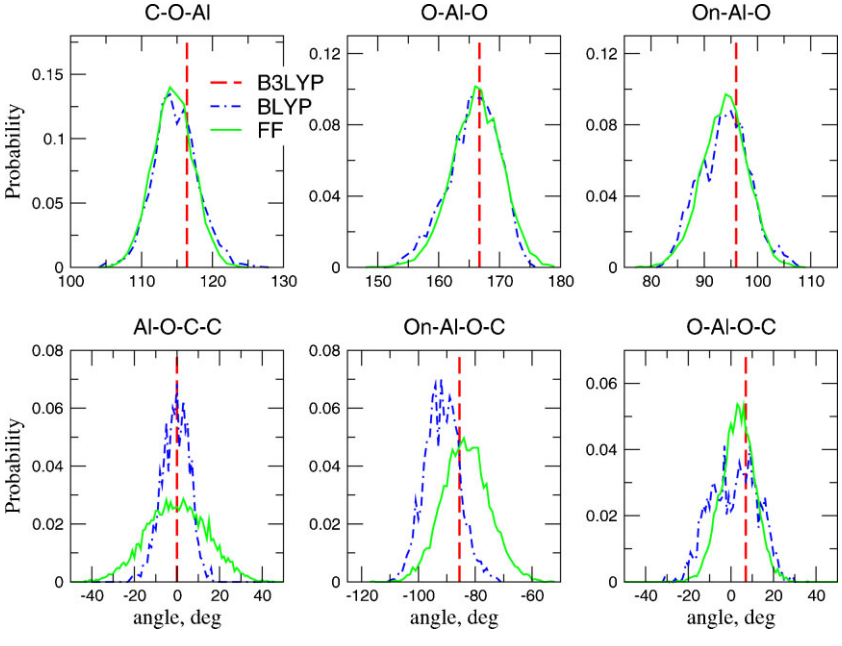

Figure 4 (online color at: www.pss-a.com) Distributions of angles and dihedrals for Car–Parrinello (BLYP) and force-field (FF) based simulations of a single molecule in vacuum. The equilibrium values obtained using B3LYP/6-311g+(d,p) functional are also indicated.

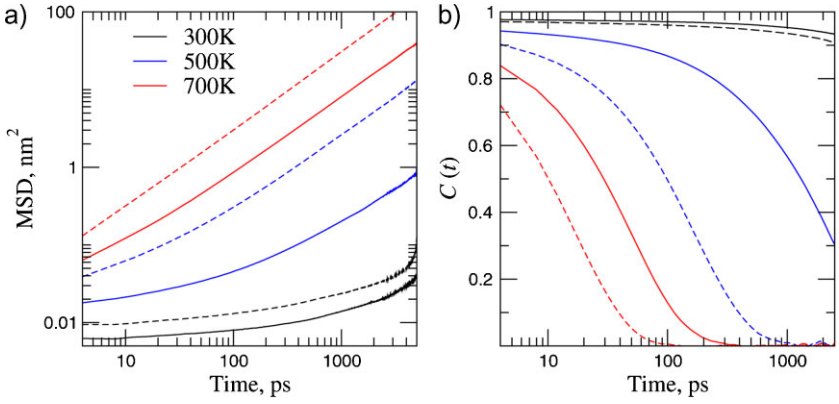

Figure 5 (online color at: www.pss-a.com) (a) Log-log plot of the mean squared displacement of the center of mass of Alq_3 molecules for a set of temperatures. (b) Correlation function of a Alq_3 molecular orientation, defined as a normal vector to the plane containing the three oxygens. Solid line: OPLS force field. Dashed line: Williams 99 force-field.

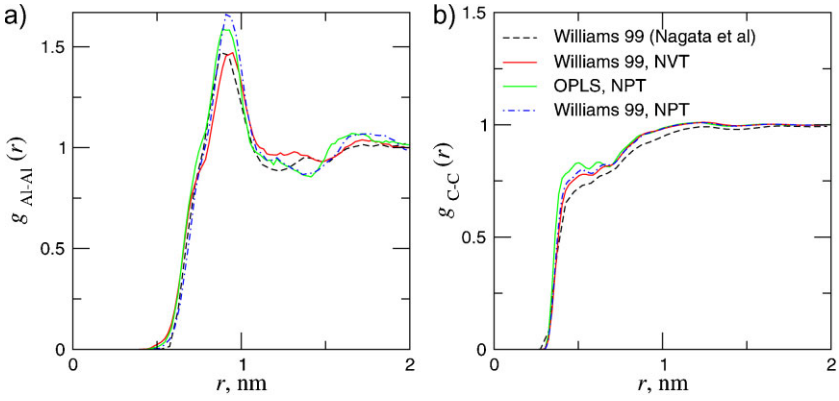

Figure 6 (online color at: www.pss-a.com) (a) Al–Al and (b) C–C radial distribution functions for OPLS and Williams 99 force fields obtained after equilibration in NPT ensemble. For comparison, results of NVT simulations (note different density) [5] are also shown.

these two curves are compared for a fixed density of [5]. On the other hand, if the systems are equilibrated in the NPT ensemble (which results in higher density), radial distribution functions have a more pronounced structure (better resolved peaks) both for OPLS- and Williams 99 based force fields. The difference between the two force fields is small. One can conclude that the radial distribution function is not an optimal measure of molecular packing, due to its limited sensitivity.

Two other microscopic quantities are known from experiments: the density of amorphous Alq_3 at ambient conditions and its glass transition temperature [16, 18]. The density *versus* temperature plot is shown in Fig. 7a. One can see that the system density strongly depends on the Lennard–Jones parameters (and does not change if we substitute ESP charges derived from the B3LYP- with MP2-based electron density). One can see that OPLS predicts a higher density than Williams 99 and it is also closer to the experimental values. Densities used in previous simulation studies by Y. Nagata et al. [5] (density is mentioned in the paper) and J. Kwiatkowski et. al. [4] (density is calculated using number of molecules and the box size specified in the paper) are also shown for comparison.

To estimate the glass transition temperature we calculated the volume of the simulation box as a function of temperature. These dependencies are shown in Fig. 7b. By performing a linear fit of the low and high temperature parts of the curves one can find the intersection point which provides an estimate of the glass transition temperature [19].

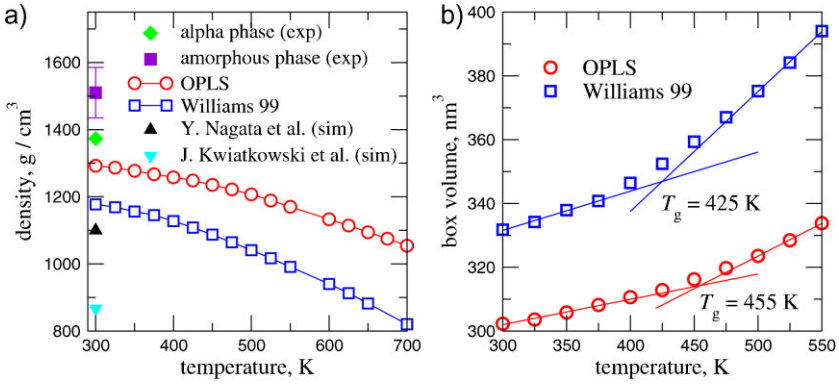

Figure 7 (online color at: www.pss-a.com) (a) Density *versus* temperature for OPLS and Williams 99-based force-fields together with experimental results: amorphous density is taken from [16], alpha-phase density is taken from [17]. Density used in previous studies by Y. Nagata et al. [5] and J. Kwiatkowski et al. [4] are also shown. (b) Volume of the simulation box *versus* temperature for amorphous Alq_3. Intersection of two fitting lines is used to predict glass transition temperature, which is estimated to be 455 K for OPLS and 425 K for Williams 99 force field. Experimental value is 448 K [18].

The latter is estimated to be 455 K for OPLS and 425 K for Williams 99 force field. Experimental value is 448 K [18], which is again closer to the OPLS-predicted value.

Summarizing, we can conclude that the OPLS-based force field performs better for the amorphous Alq_3 films than the Williams 99 force field by predicting closer to the experimental values of density and glass transition temperature.

3 Charge transport To relate microscopic molecular arrangement to charge carrier mobility we used a thermally-activated charge hopping formalism with the rate of hops given by Marcus theory [3, 20–23]. The higher the rate, the faster the charge carrier (either hole or electron) moves between neighboring molecules, and the higher the mobility. The transfer rate ω depends, in the framework on Marcus theory, on two key parameters: the reorganization energy λ and the transfer integral J [24].

The reorganization energy λ, which does not depend on the relative positions/orientations of neighboring molecules, was computed as the sum of the relaxation energies for neutral and positive radicals following [21] using B3LYP functional with a triple zeta split basis set, 6-311g+(d,p), using the GAUSSIAN 03 [10] program. The computed values for the reorganization energies are $\lambda_h = 0.23$ eV and $\lambda_e = 0.28$ eV.

The transfer integral J describes the probability of electron tunneling between two neighboring molecules. We compute it using the intermediate neglect of differential overlap level of theory (ZINDO) as described in [25]. Molecular orbitals are calculated using the GAUSSIAN 98 package [26]. Since the transfer integral is related to the molecular overlap, it is very sensitive to relative orientations and positions of the neighbors. The corresponding HOMO and LUMO orbitals are shown in Fig. 8a. Note that ZINDO predicts that the LUMO is localized on one of the arms, while DFT calculations in [4], as well as our MP2 calculations (Fig. 8a) show that the LUMO is delocalized over two of them. Different localization will of course affect charge dynamics, especially the ratio between the hole and electron mobilities, since the delocalization leads to the less pronounced dependence of transfer integrals on the mutual orientation of neighbors.

However, here we do not aim at a quantitative description of charge dynamics, since we anyway ignore several essential ingredients required for its correct description, such as diagonal disorder as well as electrostatic and polarization contributions to it. Our main goal is to understand how the change of morphology influences charge carrier mobility. Hence, here we analyze only the hole transport, since all three first-principles methods predict similar localization pattern for HOMO.

For charge dynamics simulations amorphous morphologies containing 4096 molecules in a cubic box were prepared using both OPLS and Williams 99 force-fields and the aforementioned equilibration procedure. The size of the cubic box was 13.4263 nm, the length of the KMC run was 10^{-5} s, and the mobilities were averaged over ten starting points. A cut-off of 15 Å was used to calculate the hopping rates between neighboring molecules.

We first have a look at the probability distributions of the total hopping rate away from a molecule, which is shown in Fig. 8b. One can notice that the distribution that corresponds to the OPLS force-field is shifted to higher values of transfer integrals compared to the Williams 99 force-field. This is expected, since the OPLS force field predicts more dense molecular packing.

Charge carrier mobilities were calculated by monitoring the projection of the charge velocity on the field direction. The simulations were done for a single charge diffusing in an external field through the configuration of one molecular dynamics snapshot with periodic boundary conditions applied in all directions. The mobility was calculated as $\mu = v/E$, where v is the averaged over a hundred different starting positions for every frame velocity of the charge carrier along the field E.

The calculated hole mobilities are μ^{h}_{OPLS} 3.7×10^{-3} and μ^{h}_{W99} 1.7×10^{-3} $cm^2\,V^{-1}\,s^{-1}$. Both values are several orders of magnitude higher than the experimentally measured ones: electron mobilities of amorphous Alq_3 are of the order of 10^{-5}–10^{-6} $cm^2\,V^{-1}\,s^{-1}$ [1, 27] while hole mobilities are of the order of 10^{-8} $cm^2\,V^{-1}\,s^{-1}$ [1]. The discrepancy between the experimental and calculated values is due to the fact that we ignore the energetic disorder, which can significantly influence resulting mobilities [4, 5].

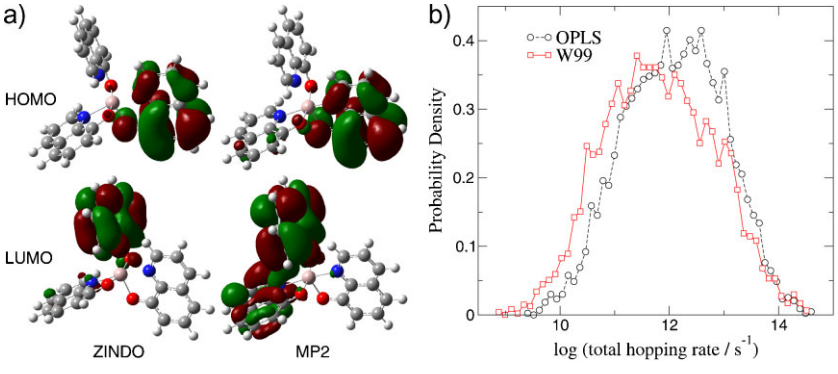

Figure 8 (online color at: www.pss-a.com) (a) HOMO and LUMO orbitals of a meridional isomer of Alq_3 calculated with ZINDO and Hartree–Fock (using MP2-optimized geometry) methods. (b) Probability distribution of the total hopping rate away from the molecule for OPLS and Williams 99 force fields. Only hole transport was considered. ZINDO orbitals were used for calculations.

4 Conclusions Intramolecular parameters of the Alq_3 force-field were refined and validated using first principles calculations. Two sets of nonbonded parameters were compared based on the OPLS and Williams 99 force field. The OPLS-based force field gives better agreement with experimentally measured values of density and the glass transition temperature of the amorphous morphology. At the same time, radial distribution functions are not very different and therefore cannot be used for a quantitative comparison of morphologies and the force fields used to generate them.

The difference in density and packing induced by different force-field parameters does not significantly affect the off-diagonal energetic disorder, leading to slightly higher mobilities in case of a more dense system (OPLS-based morphology). This implies that our method of calculating the off-diagonal energetic disorder to study charge carrier dynamics is quite robust for the case of amorphous materials.

The predicted hole mobility is much higher than the experimentally measured one because we ignore the diagonal disorder. The molecule has a large dipole resulting in a large diagonal disorder and reduction of the charge carrier mobility.

Acknowledgements A. L. acknowledges Eurosim Early Stage Training project of Marie Curie actions for the financial support. This work was partially supported by DFG via IRTG program between Germany and Korea and DFG grant AN 680/1-1. The authors are grateful to Yuki Nagata for sharing the data as well as to Victor Rühle, Thorsten Vehoff, Karen Johnston, and James Kirkpatrick for fruitful discussions and critical reading of the manuscript.

References

[1] S. Naka, H. Okada, H. Onnagawa, Y. Yamaguchi, and T. Tsutsui, Synth. Met. **111**, 331 (2000).
[2] W. Brütting, Physics of Organic Semiconductors (Wiley-VCH, Berlin, 2005), pp. 95–126.
[3] X. Feng, V. Marcon, W. Pisula, M. R. Hansen, J. Kirkpatrick, F. Grozema, D. Andrienko, K. Kremer, and K. Mullen, Nat. Mater. **8**, 421 (2009).
[4] J. J. Kwiatkowski, J. Nelson, H. Li, J. L. Bredas, W. Wenzel, and C. Lennartz, PCCP **10**, 1852 (2008).
[5] Y. Nagata and C. Lennartz, J. Chem. Phys. **129**, 034709 (2008).
[6] C. M. Breneman and K. B. Wiberg, J. Comp. Chem. **11**, 361 (1990).
[7] V. Rühle, J. Kirkpatrick, K. Kremer, and D. Andrienko, Phys. Status Solidi B **245**, 844 (2008).
[8] T. Vehoff, J. Kirkpatrick, K. Kremer, and D. Andrienko, Phys. Status Solidi B **245**, 839 (2008).
[9] V. Marcon, T. Vehoff, J. Kirkpatrick, Do, Ch. Jeong, Y. Yoon, K. Kremer, and D. Andrienko, J. Chem. Phys. **129**, 094505 (2008).
[10] M. J. Frisch, G. W. Trucks, H. B. Schlegel, G. E. Scuseria, M. A. Robb, J. R. Cheeseman, J. A. Montgomery, Jr., T. Vreven, K. N. Kudin, J. C. Burant, J. M. Millam, S. S. Iyengar, J. Tomasi, V. Barone, B. Mennucci, M. Cossi, G. Scalmani, N. Rega, G. A. Petersson, H. Nakatsuji, M. Hada, M. Ehara, K. Toyota, R. Fukuda, J. Hasegawa, M. Ishida, T. Nakajima, Y. Honda, O. Kitao, H. Nakai, M. Klene, X. Li, J. E. Knox, H. P. Hratchian, J. B. Cross, C. Adamo, J. Jaramillo, R. Gomperts, R. E. Stratmann, O. Yazyev, A. J. Austin, R. Cammi, C. Pomelli, J. W. Ochterski, P. Y. Ayala, K. Morokuma, G. A. Voth, P. Salvador, J. J. Dannenberg, V. G. Zakrzewski, S. Dapprich, A. D. Daniels, M. C. Strain, O. Farkas, D. K. Malick, A. D. Rabuck, K. Raghavachari, J. B. Foresman, J. V. Ortiz, Q. Cui, A. G. Baboul, S. Clifford, J. Cioslowski, B. B. Stefanov, G. Liu, A. Liashenko, P. Piskorz, I. Komaromi, R. L. Martin, D. J. Fox, T. Keith, M. A. Al-Laham, C. Y. Peng, A. Nanayakkara, M. Challacombe, P. M. W. Gill, B. Johnson, W. Chen, M. W. Wong, C. Gonzalez, and J. A. Pople, Gaussian Inc., Pittsburgh PA (2003).
[11] W. L. Jorgensen and J. Tirado-Rives, J. Am. Chem. Soc. **110**, 1657 (1988).
[12] D. E. Williams, J. Comp. Chem. **22**, 1154 (2001).
[13] R. Car and M. Parrinello, Phys. Rev. Lett. **55**, 2471 (1985).
[14] O. A. von Lilienfeld, I. Tavernelli, U. Rothlisberger, and D. Sebastiani, Phys. Rev. Lett. **93**, 153004 (2004).
[15] B. Hess, C. Kutzner, D. van der Spoel, and E. Lindahl, J. Chem. Theory Comput. **4**, 435 (2008).
[16] C. H. M. Maree, R. A. Weller, L. C. Feldman, K. Pakbaz, and H. W. H. Lee, J. Appl. Phys. **84**, 4013 (1998).
[17] M. Brinkmann, G. Gadret, M. Muccini, C. Taliani, N. Masciocchi, and A. Sironi, J. Am. Chem. Soc. **122**, 5147 (2000).
[18] K. Naito and A. Miura, J. Phys. Chem. **97**, 6240 (1993).
[19] S. W. Watt, J. A. Chisholm, W. Jones, and S. Motherwell, J. Chem. Phys. **121**, 9565 (2004).
[20] K. Senthilkumar, F. Grozema, F. Bickelhaupt, and L. Siebbeles, J. Chem. Phys. **119**, 9809 (2003).
[21] V. Lemaur, D. Da Silva Filho, V. Coropceanu, M. Lehmann, Y. Geerts, J. Piris, M. Debije, A. Van de Craats, K. Senthilkumar, L. Siebbeles, J. Warman, J. L. Bredas, and J. Cornil, J. Am. Chem. Soc. **126**, 3271 (2004).
[22] J. Kirkpatrick, V. Marcon, J. Nelson, K. Kremer, and D. Andrienko, Phys. Rev. Lett. **98**, 227402 (2007).
[23] J. Kirkpatrick, V. Marcon, K. Kremer, J. Nelson, and D. Andrienko, J. Chem. Phys. **129**, 094506 (2008).
[24] K. Freed and J. Jortner, J. Chem. Phys. **52**, 6272 (1970).
[25] J. Kirkpatrick, Int. J. Quant. Chem. **108**, 51 (2008).
[26] M. J. Frisch, G. W. Trucks, H. B. Schlegel, G. E. Scuseria, M. A. Robb, J. R. Cheeseman, V. G. Zakrzewski, J. A. Montgomery, Jr., R. E. Stratmann, J. C. Burant, S. Dapprich, J. M. Millam, A. D. Daniels, K. N. Kudin, M. C. Strain, O. Farkas, J. Tomasi, V. Barone, M. Cossi, R. Cammi, B. Mennucci, C. Pomelli, C. Adamo, S. Clifford, J. Ochterski, G. A. Petersson, P. Y. Ayala, Q. Cui, K. Morokuma, D. K. Malick, A. D. Rabuck, K. Raghavachari, J. B. Foresman, J. Cioslowski, J. V. Ortiz, A. G. Baboul, B. B. Stefanov, G. Liu, A. Liashenko, P. Piskorz, I. Komaromi, R. Gomperts, R. L. Martin, D. J. Fox, T. Keith, M. A. Al-Laham, C. Y. Peng, A. Nanayakkara, C. Gonzalez, M. Challacombe, P. M. W. Gill, B. Johnson, W. Chen, M. W. Wong, J. L. Andres, C. Gonzalez, M. Head-Gordon, E. S. Replogle, and J. A. Pople, GAUSSIAN 98, Gaussian, Inc., Pittsburgh PA, 1998.
[27] H. Murata, G. Malliaras, M. Uchida, Y. Shen, and Z. Kafafi, Chem. Phys. Lett. **339**, 161 (2001).

